Experimental Validation of a Robust H_∞ Control Method on Miniaturized Optical Image Stabilizer Prototypes

Alireza Alizadegan[1]
Department of Mechanical Engineering,
The University of British Columbia,
Vancouver, BC V6T1Z4, Canada
e-mail: a.r.alizadegan@gmail.com

Pan Zhao
Department of Mechanical Science and Engineering,
University of Illinois at Urbana–Champaign,
Urbana, IL 61801
e-mail: panzhao2@illinois.edu

Ryozo Nagamune
Associate Professor
Department of Mechanical Engineering,
The University of British Columbia,
Vancouver, BC V6T1Z4, Canada
e-mail: nagamune@mech.ubc.ca

Mu Chiao
Professor
Department of Mechanical Engineering,
The University of British Columbia,
Vancouver, BC V6T1Z4, Canada
e-mail: muchiao@mech.ubc.ca

This paper validates a robust H_∞ controller design method, experimentally, on miniaturized prototypes of the magnetically actuated lens-tilting optical image stabilizers (OISs) with product variabilities. Five small-scale OIS prototypes with product variations are constructed by three-dimensional (3D) printing. For the prototypes, the model parameters are identified based on experimental frequency response data of the prototypes. Using the identified model, a robust H_∞ controller is designed to guarantee the robust stability of the closed-loop system and to optimize the closed-loop performance. The experimental results reveal larger and more complex uncertainties in miniaturized OISs with mass-produced parts compared to large-scale prototypes. Despite the increased amount of uncertainties, it is demonstrated that the robust H_∞ controller still outperforms the conventional controllers in terms of robust closed-loop stability, performance, and controller order for practical implementation on a mobile phone device. [DOI: 10.1115/1.4048033]

1 Introduction

Optical image stabilizers (OISs) are electromechanical actuators used in cameras to mitigate image blur caused by hand-shake of the user. Despite its successful implementation in large-scale cameras for decades, OISs did not appear on mobile phone cameras until recently due to size and cost limitations [1–10]. In fact, as of September 2018, most of relatively large and high-end smartphones (such as iPhone XS Plus, Huawei P20 Pro, and Samsung Galaxy S9) are equipped with OISs. To further popularize OISs in not only large and high-end smartphones but also in standard mobile phones, it is critical to achieve miniaturization and low-cost manufacturing for OISs.

To deal with size and cost challenges, conceptual design of a novel magnetically actuated lens-tilting OIS was proposed in Ref. [11], which offers lower cost than recent piezoelectric actuators [12,13]; however, product variabilities in micromanufacturing of OISs were not considered. To address this issue, robust controller design methods have been introduced [14] and validated by a set of large-scale prototypes [15–17]; however, validation by the large-scale prototypes had limitations. First, applicability of robust H_∞ control to large-scale prototypes does not guarantee its applicability to miniaturized OISs because their parameter values are significantly different from the large-scale prototypes. Second, the physical product variabilities in the miniaturized OISs were mimicked by intentional beam width variations in the large-scale lens platforms, which might not be realistic enough. Moreover, the moving-magnet actuators and the base were custom-made and used commonly across all lens platforms, while it is expected that the miniaturized OISs be manufactured independently by industry-quality mass-produced parts. In other words, product variations appear in not only the lens platforms but also the actuators. Finally, many of the errors present in micromanufacturing were not considered in the previous work. For instance, in the large-scale prototypes, the permanent magnets were installed on the stainless steel lens platform by magnetic force with a good accuracy; however, in miniaturized OISs, the permanent magnets should be attached to the lens platform by glue that adds significant variabilities in the air-gap and coil-magnet misalignments. There are many other variabilities such as tolerance of the specific manufacturing method, pillar residues, curing, and other postprocessing that leads to clogging and product variabilities. Therefore, it is necessary to validate applicability of the robust H_∞ controller design method in batch-fabricated miniaturized OISs prototypes.

In this paper, the robust H_∞ controller design method proposed recently in Ref. [16] is validated by applying it to five independently fabricated miniaturized OIS prototypes containing industry-quality mass-produced parts. More specifically, the multimodel uncertainty modeling and robust H_∞ controller design method is applied to miniaturized OIS prototypes to guarantee closed-loop stability and optimize closed-loop performance considering product variabilities. Performance of closed-loop systems equipped with the designed robust H_∞ controller is compared with performance with the μ-synthesis controller in an experimental setting in both time and frequency domains.

2 Miniaturized Optical Image Stabilizer Prototypes

Miniaturized prototypes are fabricated based on OIS conceptual design in Ref. [11]. Figure 1 shows a schematic of the design layout for miniaturized OIS. The lens is to be mounted on a monolithic flat structure referred to as the lens platform. The lens platform encompasses a plate supported by four folded beams connecting the plate to the base. The folded beams provide sufficient stiffness for tilting of the plate about x- or y-axis. Tilt actuation is achieved by four moving-magnet actuators installed in four corners of the device, marked by 1–4 in equal distances from central axes. Each moving-magnet actuator consists of a pair of coil and magnet. Magnets are attached to the lens platform, whereas coils are fixed to the base. Actuation is achieved by forces generated on each magnet in response to the magnetic fields created by the current in its corresponding coil. The tilt angle of the lens platform is measured using a retro-reflective sticker and a laser Doppler vibrometer (LDV) for the prototypes. The development of platform's tilt angle sensors suitable for practical implementations is beyond the scope of this paper.

Figure 2 shows the miniaturized OIS prototypes built in the lab. The size of the prototype is compatible with generic mobile phone dimensions. The lens platform is made of PlasWHITE photopolymer and fabricated using a three-dimensional (3D) printer in

[1]Corresponding author.
Contributed by the Dynamic Systems Division of ASME for publication in the Journal of Dynamic Systems, Measurement, and Control. Manuscript received October 17, 2019; final manuscript received August 3, 2020; published online August 28, 2020. Assoc. Editor: Bin Xian.

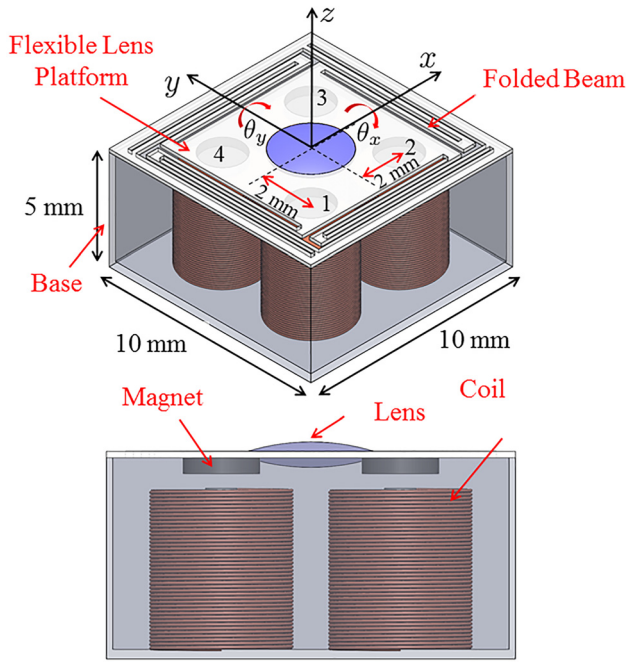

Fig. 1 Mechanical design of the miniaturized OIS [1]

batch. The lens platform is installed on a base of the same material by tolerance fitting. The coils and magnets are both commercial and mass-produced. The coils are held stationary by tolerance fitting to cylinders created in the base. The magnets are attached to the lens platform using a general-purpose glue. The numeric values for design parameters of the moving magnet actuators are compared in Table 1 with parameters proposed for the conceptual design in Ref. [11]. Even though there are minor differences in parameter values, it is expected that the results obtained from this experiment can be a good indicator of the OIS performance for the real products.

As far as image stabilization is concerned, the OIS's goal is to tilt the lens platform about either *x*- or *y*-axis to a desired angle to counteract hand-shake effects. A general control system configuration as shown in Fig. 3 was proposed in Ref. [11] to achieve this control goal.

The hand-shakes disturbances are detected by the gyrosensor of the mobile phone and integrated once to obtain the tilt angle of the camera due to handshake. The camera angle is used to calculate, in "signal processor" block in Fig. 3, the desired tilt angle of the lens that compensates for the tilt angle of the camera. The error signal is acquired by subtracting the measured tilt angle from reference tilt angle. Based on the error, the controller sends appropriate current commands to four coils in order to tilt the lens platform to minimize tracking error. In addition to tracking error minimization, sufficient stability margin should be considered to account for modeling errors, and high-frequency controller gain should be limited to avoid actuator saturation due to sensor noise amplification.

Table 1 Parameter values of the moving magnet actuator

	Design [11]	Prototypes
Inner diameter (mm)	1.0	0.5
Outer diameter (mm)	4.1	3.3
Height (mm)	4.0	4.0
Wire gauge (AWG)	36	36
Wire turns	372	347
Diameter (mm)	2.5	1.6
Thickness (mm)	0.65	0.8
Air gap at equilibrium (mm)	0.25	1

Five miniaturized OIS prototypes, named as OIS 1–OIS 5, are built as shown in Fig. 4 to realize product variabilities. The sources contributing to product variabilities in miniaturized prototypes are more complex than large-scale ones. Even though no synthetic beam width variations are imposed on miniaturized OISs, there are numerous natural sources of variabilities in lens platform such as 3D printer's fabrication tolerances, pillar residue, and the curing postprocessing that leads to clogging of the beams. The coils and magnets used in miniaturized OISs are off-the-shelf mass-produced coils and magnets with industry-quality product variabilities. The magnets are attached by glue that adds significant variabilities in air-gap and coil-magnet misalignment compared to large-scale OISs where magnets are attached by magnetic force.

3 Uncertainty Modeling of Miniaturized Optical Image Stabilizers

To design a robust controller against product variabilities, resulting dynamics variations should be captured by a model. Figure 6 shows the measured frequency responses of OIS 1–OIS 5 with solid lines. In general, the shape of the frequency responses of miniaturized OISs is similar to simulation results (Fig. 4 in Ref. [14]) and large-scale results (Fig. 11 in Ref. [16]), because all share the same conceptual design. The bandwidth is about 300 Hz, which is compatible with simulation results and sufficiently larger

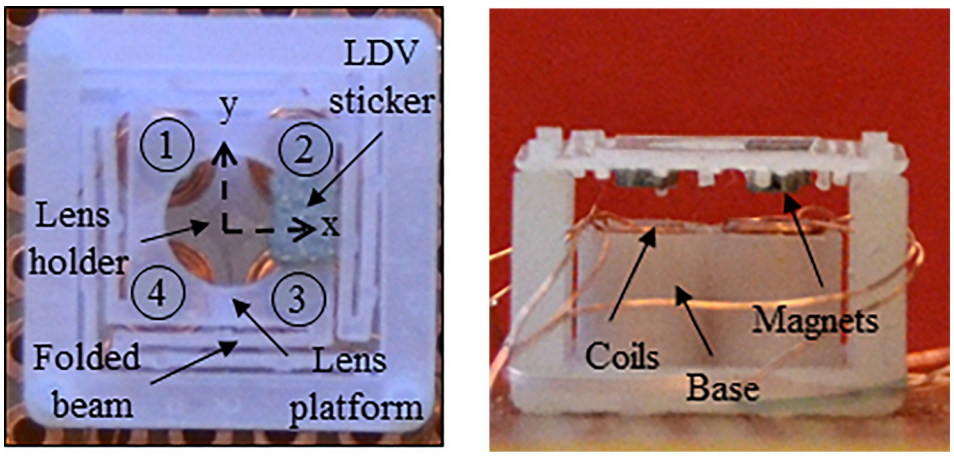

(*a*) (*b*)

Fig. 2 Miniaturized OIS prototype: (*a*) Top view and (*b*) Side view

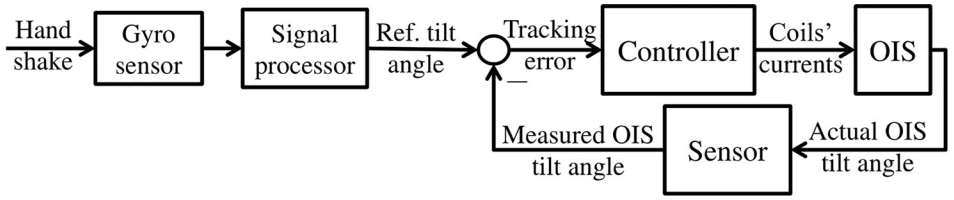

Fig. 3 Control system block diagram

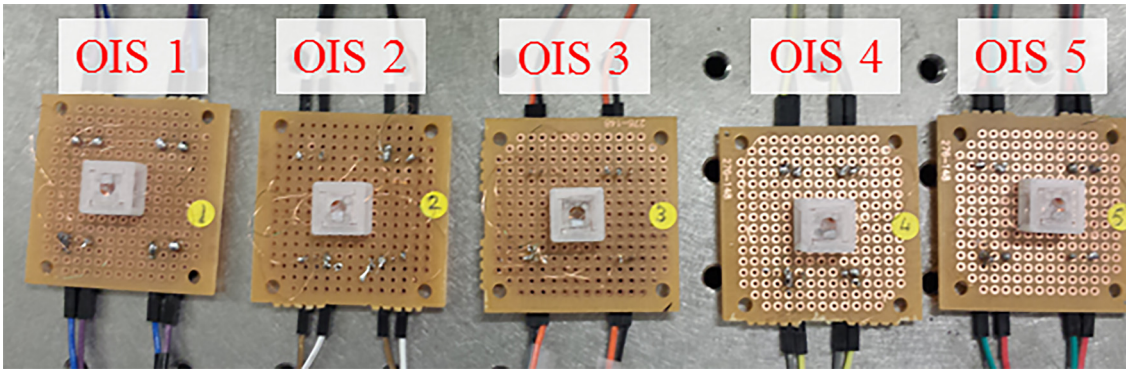

Fig. 4 Five miniaturized OIS prototypes

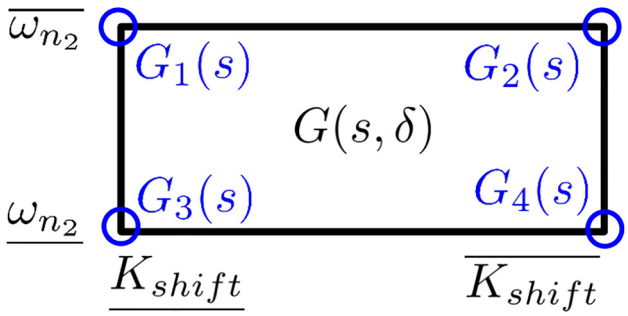

Fig. 5 Illustration of uncertainty region and multimodel

than the hand-shake disturbance bandwidth (10 Hz). Since PlasWHITE has a relatively higher damping material then stainless steel, the resonance modes of miniaturized prototypes have larger damping ratios than large-scale prototypes. There are variations in natural frequencies and DC gain due to product variabilities and coupling of shifting mode with tilting dynamics due to asymmetric actuation. The variations in frequency responses are larger and more complex than simulation and large-scale results caused by additional product variabilities. Table 2 quantitatively compares the uncertainties in dynamics parameters for miniaturized with the ones in large-scale prototypes. The uncertainties for all three main parameters are larger in percentage for miniaturized prototypes compared to large-scale ones in Ref. [16]. This increased uncertainties are due to decrease of size and use of mass-produced components.

The uncertain dynamics of OIS is expressed by a transfer function of the following structure:

$$G(s,\delta) = [G_{\text{shift}}(s,\delta) + G_{\text{tilt}}(s,\delta)]e^{-s\tau} \tag{1}$$

where G_{shift} and G_{tilt} denote the transfer functions corresponding to the coupling of shift dynamics and the tilt dynamics, respectively, and δ designates the vector of uncertain parameters representing product variabilities. The transfer functions are defined as

$$G_{\text{shift}}(s,\delta) = \frac{K_{\text{shift}}\omega_{n_1}^2}{s^2 + 2\xi_1\omega_{n_1}s + \omega_{n_1}^2} \tag{2}$$

$$G_{\text{tilt}}(s,\delta) = \frac{K_{\text{tilt}}\omega_{n_2}^2}{s^2 + 2\xi_2\omega_{n_2}s + \omega_{n_2}^2} \cdot \frac{\frac{\omega_{n_4}^2}{s^2+2\xi_4\omega_{n_4}s+\omega_{n_4}^2}}{\frac{\omega_{n_3}^2}{s^2 + 2\xi_3\omega_{n_3}s + \omega_{n_3}^2}} \tag{3}$$

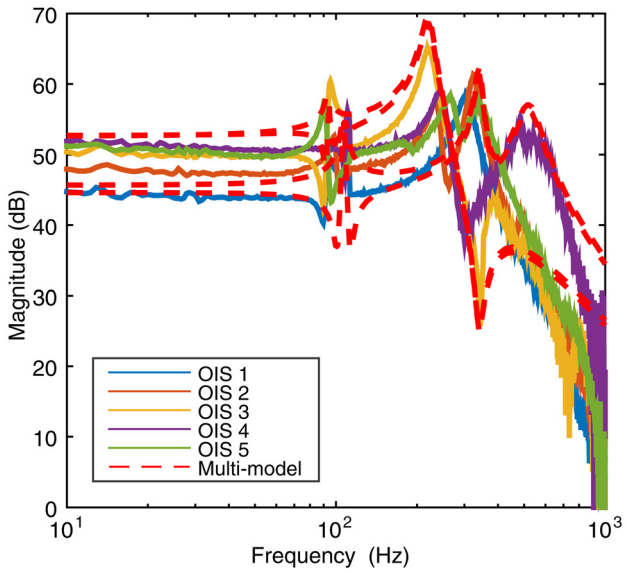

Fig. 6 Frequency responses of the proposed multimodel capturing dynamics of five prototype samples with uncertainties

Table 2 Range of uncertainties in the dynamics parameters of small scale and large scale prototypes

	Small	Large [16]
Direct current gain (dB)	[51.9, 44.7]	[13.4, 11.0]
Shift natural frequency (Hz)	[107.7, 93.9]	[67.0, 60.6]
Tilt natural frequency (Hz)	[342, 220.6]	[105.2, 96.8]

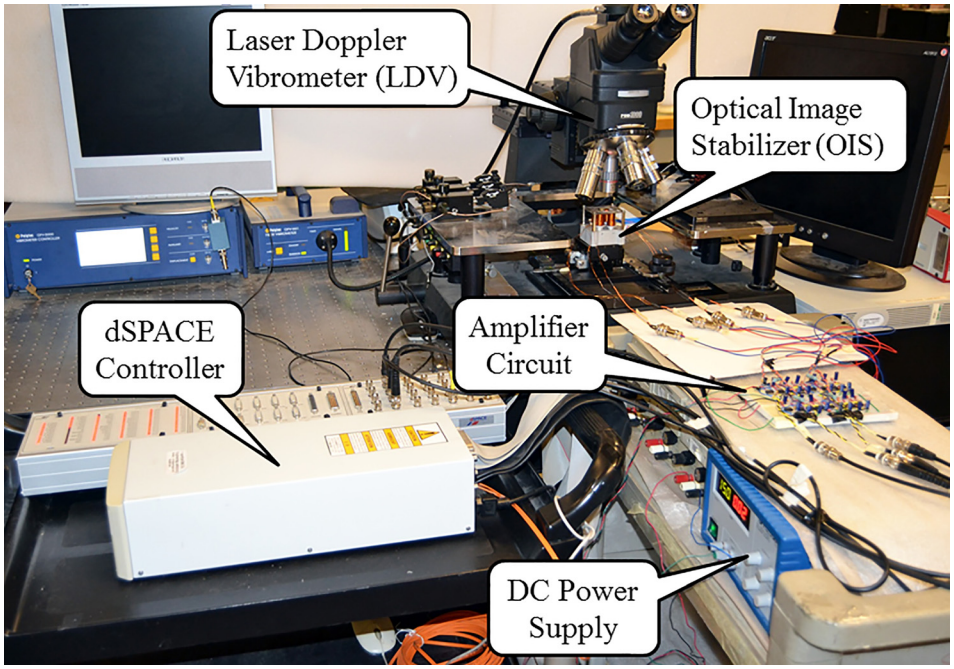

Fig. 7 The experimental setup

where ω_{n_i} and ξ_i are, respectively, natural frequency and damping ratio of the i_{th} mode. K_{shift} and K_{tilt} are DC-gains of the coupling mode and tilt dynamics, respectively.

In Eq. (1), τ is the time-delay of the amplifier circuit that will be identified experimentally and approximated by a linear transfer function using Pade approximation. Product variabilities are represented by parametric uncertainties δ in Eq. (1). Based on finite element analysis results in Ref. [16], natural frequencies and DC gains are considered uncertain while the damping ratios are assumed to be fixed. K_{shift} is considered as a standalone uncertainty parameter representing force imbalance, while ω_{n_2} is the uncertainty parameter representing beam width variations. Therefore, two independent uncertainty parameters are defined as

$$\delta := [K_{\text{shift}},\ \omega_{n_2}] \tag{4}$$

The uncertain parameters vary between an upper bound and lower bound as

$$\underline{K_{\text{shift}}} < K_{\text{shift}} < \overline{K_{\text{shift}}} \tag{5}$$

$$\underline{\omega_{n_2}} < \omega_{n_2} < \overline{\omega_{n_2}} \tag{6}$$

where underline and overline represent, respectively, the lower and upper bound of each uncertain parameter that will be identified experimentally.

Uncertainties in $\omega_{n_i}, i = 1, 3, 4$, and K_{tilt} are related to uncertainties in ω_{n_2} because they are due to the same fabrication error (beam width variations). Furthermore, this correlation can be used to reduce the number of uncertain parameters, thereby leading to a simpler controller design. The correlations are defined as

$$K_{\text{tilt}} = K^*_{\text{tilt}} \left(\frac{\omega^*_{n_2}}{\omega_{n_2}} \right)^{2c_k}, \quad \omega_{n_i} = \omega^*_{n_i} \left(\frac{\omega_{n_2}}{\omega^*_{n_2}} \right)^{c_i}, \quad i = 1, 3, 4 \tag{7}$$

where the superscript $*$ denotes the nominal values of dynamics parameters to be identified experimentally. The correlation parameters c_i, $i = 1, 3, 4$, and c_k are used to account for the increased complexity of the lens platform structure compared to a mass-spring-damper system.

Based on the two uncertain parameters, ω_{n2} and K_{tilt}, the rectangular uncertainty region is defined as illustrated in Fig. 5, where vertices denoted by δ_j, $j = 1, 2, 3, 4$, correspond to multimodel. The parameters of multimodel c_k and c_i are obtained based on frequency response data. The multimodel is compared with frequency responses in Fig. 6. It can be observed in the figure that the multimodel uncertainty model captures the variations of frequency responses.

4 Robust H_∞ Control of Miniaturized Optical Image Stabilizers

Using the method explained in Ref. [16], the following optimization problem is solved for the controller that minimizes tracking error:

$$\min_K \max_{i=1,2,3,4} ||\mathcal{T}_i(s, K)||_\infty \tag{8}$$

where $\mathcal{T}_i$ is the closed-loop system as a function of the controller $K(s)$ and index i of models in multimodel. The method employs a sequential optimization technique to design a linear time-invariant controller that minimizes tracking error, while satisfying control specifications. To compare with the robust H_∞ controller, the μ-synthesis controller is designed. To design the μ-synthesis controller, multimodel is replaced with real parametric uncertainty model. The resulting robust control problem can be solved by MATLAB Robust Control Toolbox [18] based on the μ-synthesis control theory [19].

The designed controllers are implemented on the experimental setup depicted in Fig. 7. In the experimental setup, real hand-shake signals measured by gyrosensors of a mobile phone device are used as reference signals to compensate for hand-shake effects. The tilt angle of OIS is measured by a LDV (sensor block in Fig. 7 for our experimental setup) in form of voltage signal and fed back to the controller. The actual miniaturized OIS needs to use some other sensors (e.g., hall sensors or strain gauges) that is more suitable for small scale implementation; however, this paper uses LDV for feedback because the experiment is conducted on a small-scale prototype as preliminary study. The LDV has 320 nm resolution and 20 kHz bandwidth, which is sufficient to accurately characterize dynamics of the system. The DS1103 dSPACE

Table 3 Comparison of μ-synthesis and robust H_∞ controllers on miniaturized OISs

	μ-synthesis	Robust H_∞
Designed order	289	11
Reduced order	61	10
Tracking error (deg)	0.0470 (0.0105)	0.0376 (0.0095)
Control effort (mA h)	0.9157 (0.3395)	0.8940 (0.3337)

controller board is used for controller implementation with 1 ms sampling rate. It outputs control signal in the form of voltage, which is converted to currents by an amplifier. The currents are then applied to coils to correct the tilt angle.

The closed-loop stability of controllers is analyzed experimentally on different prototypes. The designed robust H_∞ controller is compared with four conventional nominal controllers, i.e., proportional–integral–derivative, lead-lag, linear-quadratic Gaussian, and H_∞ controller. For comparison, all controllers are designed based on same control objectives and specifications defined clearly in Subsec. 2.3 of [16]. Each controller is designed based on the guidelines related to its theory to meet these objectives and specifications (see Sec. 4.2 of [16]). According to the results, none of nominal (i.e., nonrobust) controllers can stabilize the closed-loop system corresponding to all OISs because the nominal controller design methods do not take uncertainties into account. On the other hand, both robust controllers (robust H_∞ controller and μ-synthesis controller) stabilize the closed-loop system for all prototypes because the robust controller design methods take uncertainties into account and guarantee robust closed-loop stability against uncertainties in the design stage.

The robust H_∞ controller is compared with μ-synthesis controller in terms of controller order, tracking error, and control effort in Table 3. The order of the robust H_∞ controller is much smaller than that of the μ-synthesis controller since the method in Ref. [16] mathematically constraints controller order in the controller design stage. The improvements in controller order is more significant than the large-scale [16] case, where the orders of μ-synthesis controller and robust H_∞ controller were, respectively, 18 and 9. This is because as uncertainties become larger and more complex, the order of the μ-synthesis controller drastically increases. In Table 3, the values outside parentheses for tracking error and control effort are mean values over the five prototypes, while the ones inside parentheses are the worst-case degradations from the mean value. The robust H_∞ controller reduces the mean and degradation of the tracking error as well as those of the control effort compared to the μ-synthesis controller.

These improvements in the time-domain are supported by frequency-domain analysis. Figures 8(*a*) and 8(*b*) compare the robust H_∞ controller with the μ-synthesis controller in terms of the magnitude Bode plot of the transfer functions from reference to tracking error and to control input in Fig. 3, respectively. As shown in Fig. 8(*a*), the robust H_∞ controller has better error rejection compared to the μ-synthesis controller. More specifically, 0 dB crossing frequency is 24 Hz for the robust H_∞ controller, while the one for the μ-synthesis controller is 20 Hz. Besides, Fig. 8(*b*) shows that the robust H_∞ controller uses control input, which has slightly less magnitude than that of the μ-synthesis controller in low-frequency band.

The improvements achieved in tracking error and control effort can be associated with the collective effect of the following advantages of the robust H_∞ controller design over the μ-synthesis controller design. First, multimodel represents product variabilities less conservatively than real parametric uncertainty model. Furthermore, the robust H_∞ controller design provides a systematic method for obtaining a good initial guess for the solution of the nonconvex optimization problem to reduce conservatism of the controller.

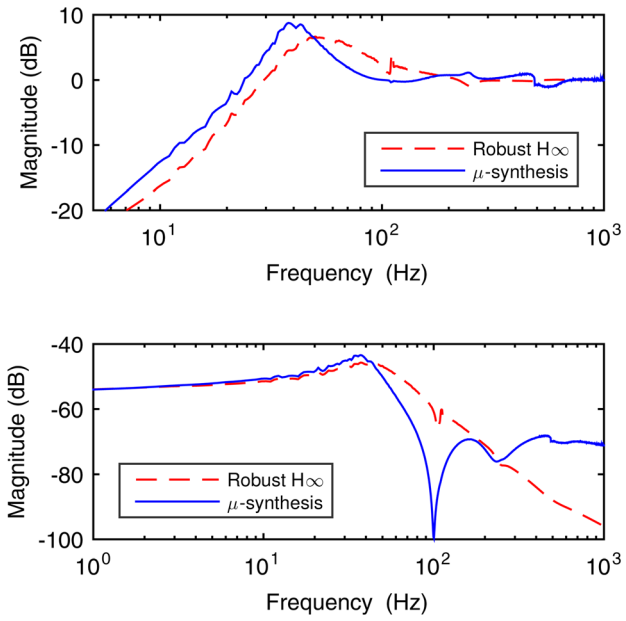

Fig. 8 Comparison between μ-synthesis and robust H_∞ controllers in frequency-domain: (*a*) Transfer function from reference to tracking error and (*b*) Transfer function from reference to control input

5 Conclusion

This paper presented an experimental validation of the uncertainty modeling and robust H_∞ control method, which were previously proposed and verified on large-scale OIS prototypes, on miniaturized OIS prototypes containing mass-produced parts. The experimental validation was carried out with five miniaturized OIS prototypes having dynamics variabilities. The frequency response tests showed larger dynamic uncertainties in miniature prototypes than large-scale ones. However, experimental results demonstrated that the robust control methods proposed and validated on large-scale prototypes in Ref. [16] can still achieve closed-loop stability for all the miniaturized OISs while conventional nonrobust controllers cannot. Besides, compared to the μ-synthesis controller, the proposed robust H_∞ control method reduced the nominal tracking error by 4.2% and its variabilities by 0.4% while also reducing control effort by 2.4% and its variabilities by 1.7%. Furthermore, the order of the robust H_∞ is reduced sixfolds compared to that of the μ-synthesis controller. In this way, the proposed robust H_∞ controller outperformed the μ-synthesis controller in terms of controller order, and closed-loop performance due to large product variabilities inherent to the miniaturized OIS prototypes. This experimental validation implies the potential of robust H_∞ control in achieving high-quality images and low cost of mobile cameras.

Acknowledgment

This work was supported by Natural Sciences and Engineering Research Council of Canada (NSERC) Strategic Partnership Grant and the Institute for Computing, Information and Cognitive Systems (ICICS) at University of British Columbia. The authors would like to thank Mr. Kaiwen Yuan of the University of British Columbia for his insightful guidance on prototyping.

Funding Data

- Natural Sciences and Engineering Research Council of Canada (NSERC) Strategic Project (Grant No. STPGP-430142-12; Funder ID: 10.13039/501100000038).

References

[1] Komori, M., and Hirakawa, T., 2005, "A Magnetically Driven Linear Microactuator With New Driving Method," IEEE/ASME Trans. Mechatronics, **10**(3), pp. 335–338.

[2] Lee, S.-K., and Kong, J.-H., 2014, "An Implementation of Closed-Loop Optical Image Stabilization System for Mobile Camera," Proceedings of the IEEE International Conference on Consumer Electronics (ICCE), Las Vegas, NV, Jan. 10–13, pp. 45–46.

[3] Chang, H. J., Kim, P. J., Song, D. S., and Choi, J. Y., 2009, "Optical Image Stabilizing System Using Multirate Fuzzy PID Controller for Mobile Device Camera," IEEE Trans. Consum. Electron., **55**(2), pp. 303–311.

[4] Yeom, D., 2009, "Optical Image Stabilizer for Digital Photographing Apparatus," IEEE Trans. Consum. Electron., **55**(3), pp. 1028–1031.

[5] Yu, H.-C., and Liu, T., 2008, "Sliding Mode Control Using Virtual Eigenvalue Method for Compact Optical Image Stabilization Actuators," IEEE Trans. Magn., **44**(11), pp. 4074–4077.

[6] Palm, R., 1994, "Robust Control by Fuzzy Sliding Mode," Automatica, **30**(9), pp. 1429–1437.

[7] Tzafestas, S. G., and Rigatos, G. G., 1999, "A Simple Robust Sliding-Mode Fuzzy-Logic Controller of the Diagonal Type," J. Intell. Rob. Syst., **26**(3/4), pp. 353–388.

[8] Yu, H.-C., and Liu, T., 2008, "Adaptive Model-Following Control for Slim Voice Coil Motor Type Optical Image Stabilization Actuator," J. Appl. Phys., **103**(7), p. 07F114.

[9] Li, T.-H. S., Chen, C.-C., and Su, Y.-T., 2012, "Optical Image Stabilizing System Using Fuzzy Sliding-Mode Controller for Digital Cameras," IEEE Trans. Consum. Electron., **58**(2), pp. 237–245.

[10] Li, T.-H. S., and Chen, C.-C., 2013, "Extended Kalman Filter Based Hand-Shake Detector for Optical Image Stabilization Using a Low Cost Gyroscope," IEEE Trans. Consum. Electron., **59**(1), pp. 113–121.

[11] Pournazari, P., Nagamune, R., and Chiao, M., 2014, "A Concept of a Magnetically-Actuated Optical Image Stabilizer for Mobile Applications," IEEE Trans. Consum. Electron., **60**(1), pp. 10–17.

[12] Yan, G. Y., Liu, Y. B., and Feng, Z. H., 2015, "A Dual-Stage Piezoelectric Stack for High-Speed and Long-Range Actuation," IEEE/ASME Trans. Mechatronics, **20**(5), pp. 2637–2641.

[13] Wang, F., Liang, C., Tian, Y., Zhao, X., and Zhang, D., 2015, "Design of a Piezoelectric-Actuated Microgripper With a Three-Stage Flexure-Based Amplification," IEEE/ASME Trans. Mechatronics, **20**(5), pp. 2205–2213.

[14] Alizadegan, A., Zhao, P., Nagamune, R., and Chiao, M., 2016, "Modeling and Robust Control of Miniaturized Magnetically-Actuated Optical Image Stabilizer," Proceedings of the IEEE International Conference on Advanced Intelligent Mechatronics (AIM), Banff, AB, Canada, July 12–15, pp. 846–851.

[15] Zhao, P., Alizadegan, A., Nagamune, R., and Chiao, M., 2015, "Robust Control of Large-Scale Prototypes for Miniaturized Optical Image Stabilizers With Product Variations," Proceedings of the 54th Annual Conference of the Society of Instrument and Control Engineers of Japan (SICE), Hangzhou, China, July 28–30, pp. 734–739.

[16] Alizadegan, A., Zhao, P., Nagamune, R., and Chiao, M., 2018, "Robust H_∞ Control of Miniaturized Optical Image Stabilizers Against Product Variabilities," IFAC Control Eng. Pract., **80**, pp. 70–82.

[17] Zhao, P., Nagamune, R., and Chiao, M., 2018, "Multiple Parameter-Dependent Robust Control of Miniaturized Optical Image Stabilizers," IFAC Control Eng. Pract., **76**, pp. 1–11.

[18] BalasChiang, G., Packard, R. A., and Safonov, M., 2007, "Robust Control Toolbox 3: User's Guide," Mathworks, Natick, MA.

[19] Packard, A., and Doyle, J., 1993, "The Complex Structured Singular Value," Automatica, **29**(1), pp. 71–109.